

PREDICTING LOADS ON A LNG CARRIER WITH CFD

Fahd Fathi
SBM Offshore | GustoMSC
Schiedam , Netherlands

Christiaan Klaij
Marin
Wageningen, Netherlands

Arjen Koop
Marin
Wageningen, Netherlands

ABSTRACT

The Current Affairs Joint Industry Project was initiated to develop the understanding and tools for the assessment of current loads on offshore structures. CFD is one of these tools requiring a good understanding of the underlying physical and mathematical models. In order to assess its suitability for the prediction of current loads on monohulls, the flow around a LNG carrier for which model scale data is available was considered. The LNG carrier, including bilge-keels and rudder, was towed at scale 1/50 in Marin's shallow water basin during the HAWAI JIP, for flow angles between 0 and 180 degrees. The measurements were shared with the Current Affairs JIP, for which the participants were invited to perform CFD computations reproducing the model test results. A number of these simulations are presented in this paper. The analysis of the results includes discussion on the grid generation as well as the numerical and physical parameters of the simulation. The comparison between experiments and computations shows that CFD can provide good qualitative predictions for the variation of force coefficients with inflow angle. The origin of the result variability between the participants is discussed and attention is drawn to the different factors influencing the quality of the simulation.

INTRODUCTION

The Current Affairs Joint Industry Project was initiated in 2007. The objective of the JIP was to develop the understanding and tools for the assessment of current loads on offshore structures. Different estimation methods were used during the JIP, namely model testing, semi-empirical formulation and Computational Fluid Dynamics (CFD) calculations. For this purpose, towing tests were performed at the Marin basin and a semi-empirical calculation tool using a wake shielding model was developed [1]. The emphasis of the project was put on both multi-column floaters and monohulls. [2] describes a specific case of multicolumn floater from the JIP, for which the different current load assessment methods were compared. One of the major outcomes of the project was the insight gained in the use

of CFD to calculate current loads. It is only recently, due to the large increase in computational power access and the improvement of numerical algorithms, that CFD became an accepted engineering simulation tool in the offshore industry. Yet, many questions with regard to its best use and related accuracy remain without a clear answer. One goal of the JIP was to shed light on some of these issues with respect to current load calculation. The research took the form a fruitful cooperation between industrial and academic partners comparing their respective approaches to the problem. Several participants were asked to perform computations on the same case. Each participant was free to choose his own modeling approach as well as CFD code. The different results were discussed and compared with experiments. The multiplicity of approaches to the problem gave its richness to the project by showing how the modeling assumptions can influence the result of a simulation. From the large amount of data gathered, of which this paper presents a small sample, best practice guidelines and recommendation were drawn.

For straight sailing ships the use of CFD methods for resistance prediction has been thoroughly studied in the Gothenburg 2000 workshop [3] for three hulls without appendages. In the Tokyo 2005 workshop [4] one of these hulls, a Very Large Crude Carrier, was considered at small drift angles (0 to 15 degrees). In this paper, we consider a LNG carrier with rudder and bilge keels in current angles from 0 to 180 degrees. During the HAWAI JIP [6,7] the current coefficients for the LNGC were measured in MARIN's shallow water basin. PIV results for a similar hull [5] show massive flow separation, even at moderate angles. Thus, the flow field is very complex and formal procedures for verification and validation such as proposed in [8,9] and used in [3,4] are still out of reach for this situation. Two participants were asked to perform flow simulations around the LNGC hull and their results are discussed in light of the comparison with model tests. The verification work was inspired from the guidelines in [10] and an informal numerical sensitivity study is presented.

The focus of the discussion is put on the computational and engineering requirements to obtain reliable results.

NOMENCLATURE

Table 1 - List of abbreviations

Abbreviation	Quantity
F _x	Longitudinal drag
F _y	Lateral lift
M _z	Yaw moment with respect to the centerline midship point
y ⁺	Non dimensional first cell height

Unless stated otherwise, all the forces and moments are non dimensional with respect to the corresponding experimental value. The values in the graphs are omitted for confidentiality reasons. The reference frame for the load projection is attached to the hull and is rotated with the heading as shown in Figure 1. With this convention, head current correspond to 180° heading and beam current to 90° heading.

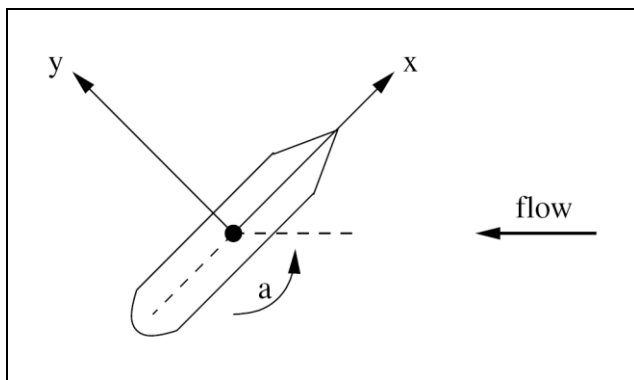


Figure 1 - Axis and rotation convention

MODEL TESTS

The model tests were performed at the Marin towing tank in Wageningen Netherlands for the HAWAI JIP. They were used as validation data for the CFD calculations. The validation was mainly performed on the global loads (moments and forces) on the hull. The model consists of a 1:50 scale model of a LNGC hull. It was towed in the tank at various angles and a 6 component measurement frame was used to record the time histories of the loading. The dimensions of the model are such that the ratio of the water depth to the draft is $WD/T=4.8$. For this value, shallow water effects might have an influence on the current forces. This question is addressed in the simulations by varying the boundary conditions of the domain. Given a basin

Table 3 - CFD code characteristics

Participant	Code Name	Code Type	Version	Discretization Method	Solver Strategy	Parallelization Method	Grid Types Supported
P1	CFX	Commercial	11.0SP1, 12.0	Finite Volume	Coupled mass & momentum Decoupled turbulence	MPI	Unstructured
P2							
P2	ReFresco	In-house	v0.9	Finite Volume	Segregated (SIMPLE)	MPI	Arbitrary Unstructured Polyhedrals

width of 15.8m, limited flow blockage from the basin side walls could be expected for some flow angles. The dimensions of the model are described in Table 2 and pictures are shown in Figure 2. In order for the free surface effects to be neglected, the towing speed was such that a very small Froude number was reached ($Fr \sim 0.04$). This resulted in a model scale Reynolds number of $1.3 \cdot 10^6$. The hull features bilge keels, a rudder and the main propeller. Between two different tows the tank was left at rest for 10 minutes to allow for background turbulence to dissipate.

Table 2 - Hull main particulars at prototype scale

Lpp	274.0 m
LOA	287.6 m
B	44.2 m
T	11.0 m
Displacement	99,210 t
CB	0.729
Capacity	135,000 m ³
Scale	50

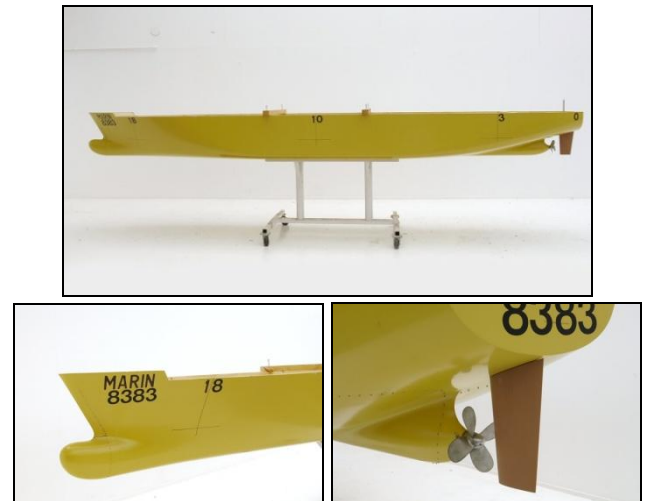


Figure 2 - Test model pictures

CODE DESCRIPTION AND GRID GENERATION

The CFD calculations were performed by two participants to reproduce some of the model test results. The variability of approaches was characterized by the different codes used, the computational meshes and the domain definition. The two participants are denoted 'P1' and 'P2'.

Flow solvers

Two different viscous-flow codes have been used in this study: a commercial package, CFX [11] and an in-house code, ReFresco [12]. Both codes solve the unsteady RANS equations, together with eddy-viscosity-based turbulence models. They also have LES capabilities which were not investigated in this

project. While ReFresco is a proprietary development which was only used by one participant, CFX was available and used by both participants.

Table 3 summarizes the codes used and their main characteristics. They all employ the finite volume discretization method along with MPI parallel scheme and sub-domain decomposition. CFX is a coupled solver, solving mass and momentum conservation in a single set of algebraic relations using a pseudo transient approach for the solver under-relaxation. The advection terms are discretized with the so-called "High resolution" scheme which is a local blending between first order upwind and second order central differences. Its order is therefore formally comprised between 1 and 2. ReFresco is a segregated code, solving mass and momentum separately, with the coupling carried out iteratively using a pressure correction scheme (SIMPLE). The advection terms are discretized with a QUICK scheme which is at least second order in an unstructured grid. While ReFresco can deal with any kind of unstructured elements (any polyhedral cell type) and hanging nodes, CFX can only handle more general cell types (hexahedrons, tetrahedrons, prisms and pyramids).

Unless stated otherwise, the SST turbulence model described in the turbulence model variation study is used by both participants.

Grid generation

The computational meshes were created from a 3D CAD model of the hull used in the model tests. The geometry features the bilge keels and the rudder but no propeller. The bilge keels were represented differently by the participants. While P2 kept the original triangular sectional shape, P1 modeled the bilge keels as flat plates. Each participant was free to choose his own grid generation method, domain shape and boundary conditions. The RANS formulations of the flow solvers and especially the Low Reynolds turbulence model used were driving the mesh generation in the boundary layer zone.

Participant P1 generated two types of grid using the meshing software ICEM CFD. The first one is a block structured type exclusively composed of hexahedrons. The mesh structure forms an O-grid blocking around the hull. The bilge keels and rudder also have their own O-grid blocking. The computational domain dimensions are set accordingly to the basin wall dimensions. The side walls are treated as a free slip wall. 3 hull headings have been considered, 180° (head current), 135° (bow quartering current) and 90° (beam current) each one with a mesh adapted to the flow direction. The external mesh blocks are rotated and the interior blocks are adapted by curving the edges. A final smoothing is applied to the hexahedral mesh. The boundary layer captured by the O-grid structures have a spanwise cell expansion factor of 1.25. The first cell height is set to ensure $y^+ < 1$. Pictures of the mesh are shown in Figure 3.

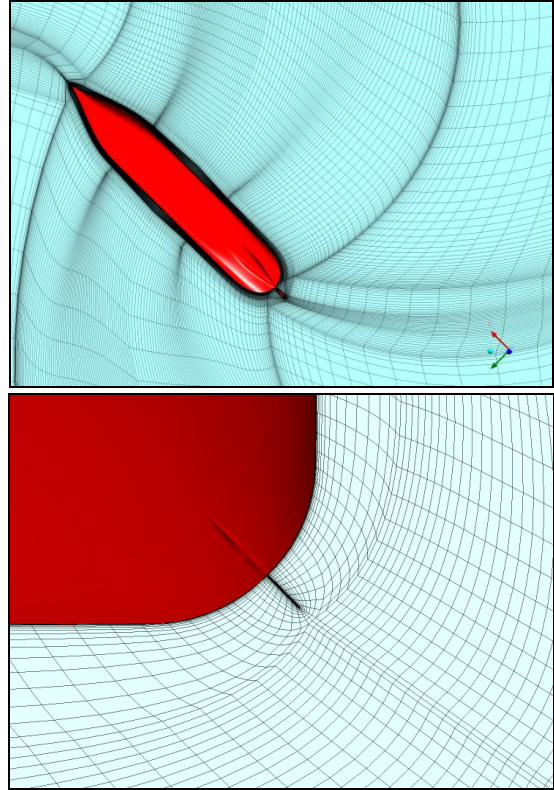
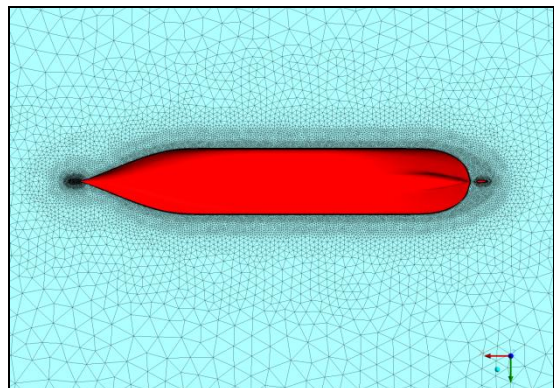


Figure 3 - P1 structured mesh (ICEM) pictures: top view 135° heading - midship plane 180° heading – Bilge keels detail

The second type of mesh generated by P1 is an unstructured tetrahedron mesh. In this case, the side walls do not respect the basin dimensions. The domain is a circular cylinder around the hull. The depth of the domain is similar to the basin one and the cylinder diameter corresponds to 5 Lpp. With this approach, the same grid can be used for all headings simply by changing the flow direction. The mesh is refined around the hull. Further refinement is set around the bow, bilge keels and rudder. The boundary layer is captured with an inflated layer of prismatic cells with a span wise expansion factor of 1.25. The basic mesh is generated using an octree algorithm. Variations on the unstructured mesh generation method are discussed in the next section.



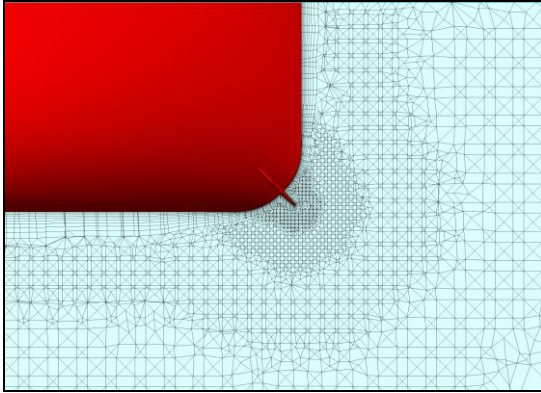


Figure 4 - P1 unstructured mesh pictures: top view - Bilge keels detail

Participant P2 followed two different approaches to generate block-structured grids. For the first one, he used ICEM CFD to create a mesh adapted to the hull heading. To reduce the grid generation effort, a block structured grid is first created for half the ship in a narrow domain. Secondly, the grid is mirrored to get a symmetric grid for the entire ship in a narrow domain. Finally, the grid is rotated to the desired angle and the narrow domain is connected to the basin walls. The procedure is schematized in Figure 5. When changing the heading, only the (simple) rectangular blocks between the narrow domain and the basin walls have to be altered and the (complex) mesh around the ship can be maintained. The typical grid size is about 1.8M cells.

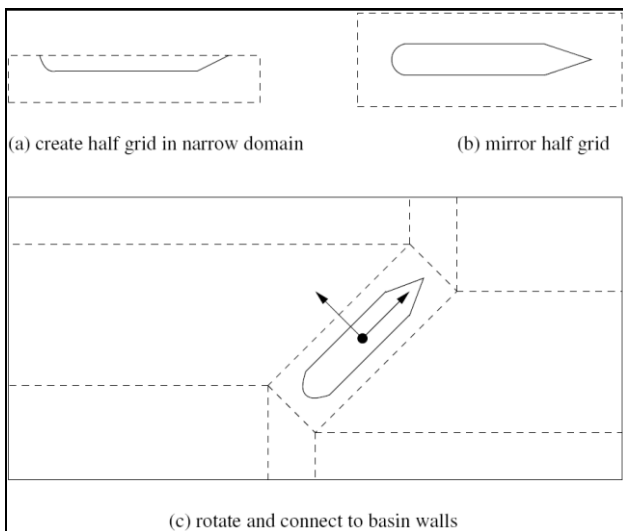


Figure 5 – Meshing process used by P2

Additionally, a second approach is considered which disregards the basin side-walls by using a wide cylindrical domain of diameter $4 L_{pp}$. Similarly to P1 this was done in order to use the same mesh for every heading. The meshing package GridPro was used to generate the structured grid for the cylindrical domain, resulting in a grid size of about 4.2M cells. The code ReFresco determines which parts of the outer

boundary should be fitted with an inflow or outflow boundary condition, based on the specified flow direction. The distance to the basin bottom is respected in both grid generation approaches. However, unlike for the ICEM mesh, the bottom is treated as an opening with imposed constant hydrostatic pressure. This is done in order to compute the current coefficients of the hull free of blockage effects. GridPro mesh planes are shown in Figure 6.

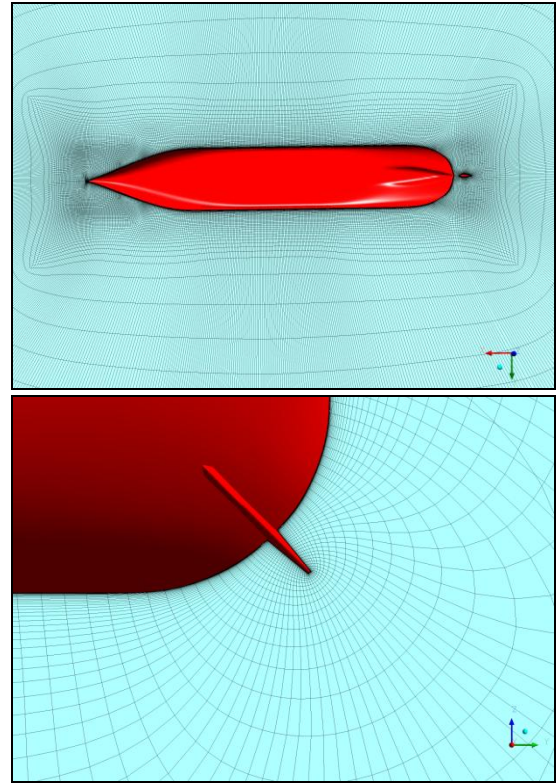


Figure 6 – P2 structured mesh (GridPro) pictures: top view - Bilge keel detail

Apart from the side and bottom walls, both participants use the same boundary conditions. A uniform velocity field is specified at the inlet boundary and for the outlet, the average pressure is imposed. Since the towing tests were performed at low Froude number, free surface effects are neglected and the simulation is monophasic. The free surface is modeled as a plane with symmetry condition. A summary of all the meshes generated is given in Table 4.

Table 4 – Computational meshes used in the study

Participant	Mesh type	Mesh size (nodes)	Generation package	y+	Side walls
P1	Block structured	2.20 - 3.08 M	ICEM CFD	<1	Basin dimensions
	Unstructured	2.82 M	ICEM CFD	<1	Cylinder 5*Lpp
P2	Block structured	1.8 M	ICEM CFD	<1	Basin dimensions
	Block structured	4.2 M	GridPro	<1	Cylinder 4*Lpp

NUMERICAL SENSITIVITY STUDIES

Iterative convergence

The calculations are considered iteratively converged after stabilization of both the equation residuals and the global forces and moments. The RMS residual convergence is shown for the 140 heading, for different set-up in Figure 7. In all the simulations, the residual levels are reduced by several orders of magnitude.

The comparison of P1 results shows similar levels of residuals for both the structured and unstructured grids. However, as shown in Figure 8, for fully detached flows such as the 90⁰ heading, the local distribution of the residuals in the domain is quite different between the two types of grid. The solver equation residual isosurface in Figure 8 (right) is typical of what was obtained for all the unstructured meshes computed regardless of the type of refinement. In comparison, the residuals presented in Figure 8 (left) for the structured mesh are much more limited. The high residuals of the unstructured mesh are present in areas with large flow gradients. They affect the global accuracy of the simulation. This highlights the influence of the mesh type on the solver accuracy. Flow aligned hexahedral elements induce less numerical diffusion than uniformly distributed tetrahedrons. Although the structured grids are more complex to generate when compared to unstructured, they procure improved numerical accuracy to the simulation.

P2 results show that using the same grid, both the CFX and ReFresco residuals are reduced by several orders of magnitude and stabilized. When using the same solver ReFresco, the GridPro grid which is globally smoother than the ICEM grid results in lower residuals.

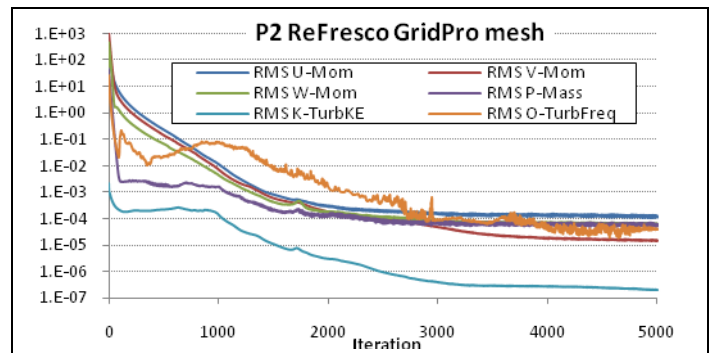
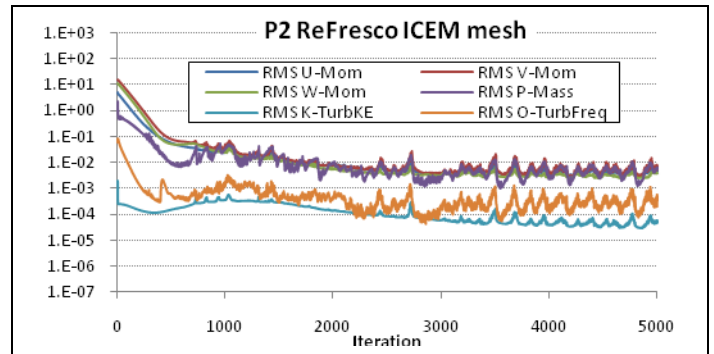
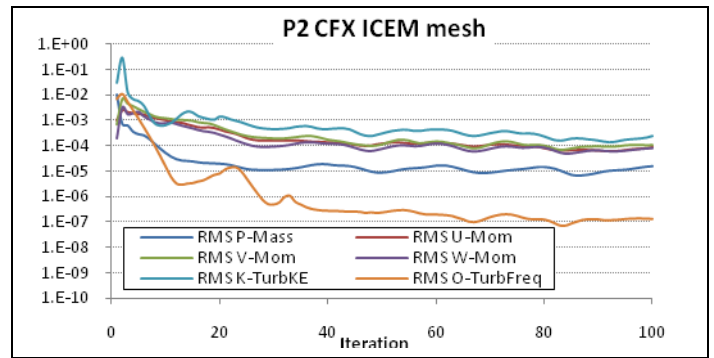
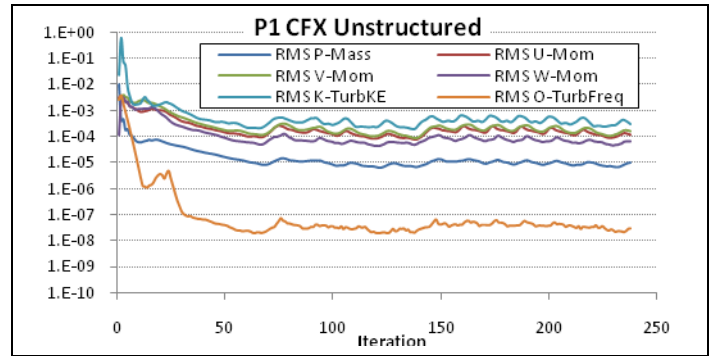
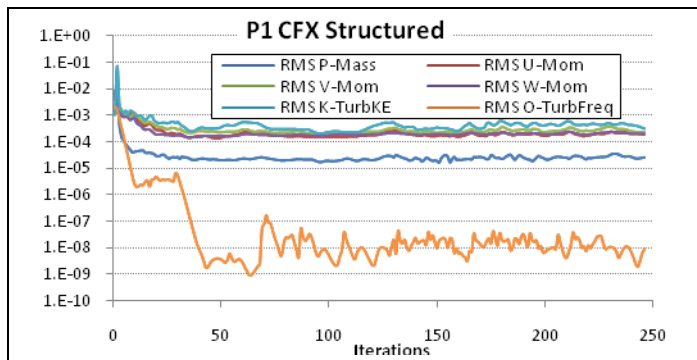


Figure 7 - Solver iterative residual convergence for different set up at the 140⁰ heading

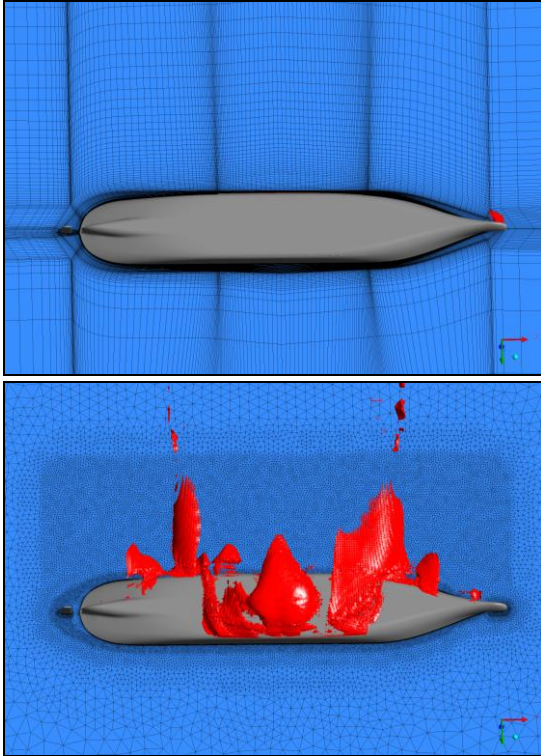


Figure 8 – Momentum equation residual isosurface at $5 \cdot 10^{-5}$ for the 90° heading (P1 CFX): structured mesh - refined unstructured mesh

Structured mesh convergence

The mesh refinement studies are inspired by the formal procedures described in [3,4]. Given the complexity of the flow, the complete analysis for all angles is out of reach. P1 performed the grid convergence study using a uniform geometric mesh refinement on the structured grid for the 180° heading. The finest grid was first generated. Its size was derived from engineering considerations aiming at a computation time of less than 24 hours on a common desktop quadcore for the steady case. A uniform coarsening of the mesh was then performed to generate the intermediate and coarse meshes. The refinement ratio between two subsequent meshes is $\sqrt{2}$. The mesh sizes and corresponding y^+ are given in Table 5. Mesh convergence is based on the longitudinal drag which is the only significant current loading for this heading. As shown in Figure 9, the two components of the drag, the wall shear force and the integrated hull pressure, evolve differently with the mesh refinement. The skin friction is the main drag component, amounting to 86% of the total force. It exhibits small amplitude variations of less than 0.5% with mesh refinement. Its evolution shows that the asymptotic convergence range has not been reached. This can be attributed to the change in first cell height which influences the turbulence modeling and therefore the wall shear forces. However, the relative changes are small enough to be neglected. The integrated pressure drag on the hull exhibits a more converging pattern with respect to mesh refinement. The

variation amplitude is significantly larger than for the skin friction. This follows the usual observation that the pressure forces are more affected by the mesh refinement than the wall shear.

Table 5 - Structured mesh refinement study by P1

	Coarse	Medium	Fine
Grid size	375 422	889 514	2 275 046
y^+ (Mean/Max)	1.50 / 1.89	1.01 / 1.55	0.70 / 1.12
ε (frictional)	-	-0.079 %	-0.459 %
ε (pressure)	-	26.69 %	9.75 %

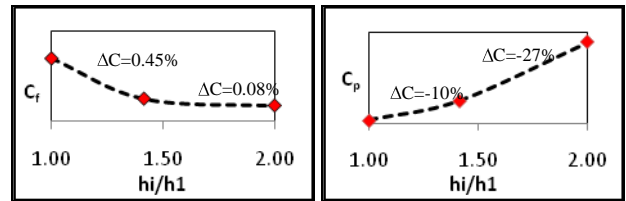


Figure 9 - Drag convergence pattern with the mesh refinement. h_i/h_1 is the cell size divided by the finest cell size: friction drag – pressure drag

P2 performed a similar mesh convergence study for the 140° heading with ReFresco using three different GridPro meshes. The coarse grids are generated by successive geometric coarsening of the finest mesh with ratio $\sqrt[3]{2}$ in three directions. The largest grid amounts to 8.7 M cells. It required the use of a large number of CPU cores and significant computer memory. The setup used corresponds to the situation for which the bottom wall is treated as an opening therefore removing the flow blockage effects. The mesh sizes and resulting loads are reported in Table 6. Comparison of lateral lift shows that the grid dependence of the results is relatively limited and that a good mesh convergence level has been reached. The deviations from model test results are relatively large and increase with mesh refinement. Most of the deviation can be attributed to the absence of flow blockage due to the open boundary conditions. This aspect is addressed in the blockage effect study. Given the small grid dependency, the medium sized grid was used for all the remaining calculations.

Table 6 - Structured mesh refinement study by P2

	Coarse	Medium	Fine
Grid size	2 173 415	4 367 719	8 735 293
y^+ (Mean/Max)	0.047 / 0.4	0.036 / 0.34	0.027 / 0.30
F_y	0.737	0.729	0.719
ε	-	-1.32%	-1.46%

Unstructured mesh convergence

For the unstructured mesh rather than using a global refinement parameter, P1 preferred the use of local refinement boxes. The 90° heading was selected for this study in order to check the

influence of the cell size on the capture of the flow recirculations. A standard unstructured mesh was generated with standard refinement parameters around the hull and the appendages as shown in Figure 10. Two different types of refinement boxes were then set around the hull in addition to the standard setup. The first features an extended and rather coarse refinement. The second features a more localized and finer refinement close to the hull. Both refinements are illustrated with their transverse midship plane in Figure 10. In order to keep the grid size of the same order as the initial mesh, the number of boundary layer cells (15 cells instead of 25 originally) was decreased by increasing the first cell height and decreasing the total boundary layer mesh height. These meshes are called high y^+ , as opposed to the initial low y^+ mesh. For high y^+ values the SST turbulence model implementation in CFX automatically switches to the use of scalable wall functions to compute the velocities at the first cell depending on the wall distance. This is the result of the blending between $k-\omega$ and $k-\epsilon$ model which is at the heart of the SST formulation. The turbulence model is therefore still considered valid for the high y^+ mesh. The boundary layer mesh coarsening was intended under the assumption that for quartering and beam current, the boundary layer plays a minor role on the loads which are dominated by pressure forces. In order to check this assumption, a large mesh featuring the initial boundary layer mesh as well as the extended refinement box was generated. All the different grids and their corresponding computed lift force are summarized in Table 7. The comparison is performed on the lateral drag which is the dominant component of the current forces.

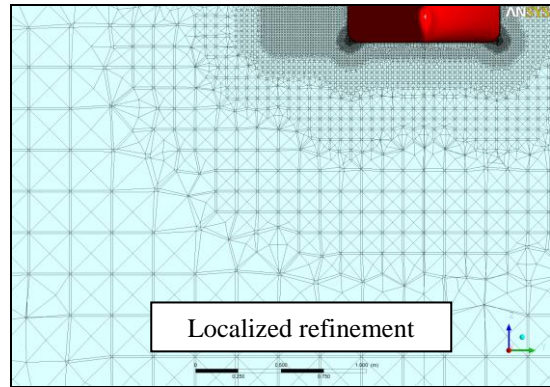
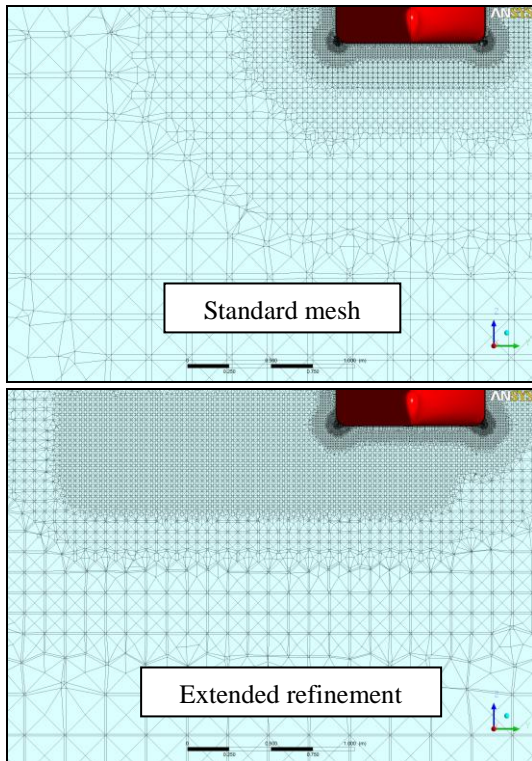


Figure 10 – Midship planes for the different unstructured meshes.

Table 7 - mesh sizes and computed loads for the mesh convergence study at 90^0

Mesh type	mesh size (nodes)	F_y	y^+ (Mean/Max)
Standard Octree with low y^+	2,821,913	0.878	0.9 / 1.42
Large refinement box with low y^+	3,993,839	0.871	0.9 / 1.41
Large refinement box with high y^+	2,800,899	0.820	8.5 / 17.5
Small refinement box with high y^+	2,695,439	0.818	7.8 / 17.0
Structured mesh	3,080,502	1.017	0.7 / 1.42
Model test	-	1.000	-



The loads from the unstructured low y^+ meshes are relatively close regardless of the presence of the refinement box. Similarly, the loads from the unstructured high y^+ meshes are also close to each other. The structured mesh stands out with the best agreement with the model test results. This comparison of the forces shows that the boundary layer mesh has a strong influence on the forces while the refinement does not affect them as much as expected. This may be due to the too poor level of unstructured refinement although it adds more than 1M nodes to the original grid. As a consequence of the difference with the results on the structured mesh which is taken as the reference, the unstructured mesh simulations cannot be considered grid independent. The reason for the influence of the boundary layer mesh coarsening on the forces are certainly related to the use of wall functions at the surface of the hull. They affect the flow detachment along the smooth curvature surfaces such as the bow and the bilge. This is in contradiction with the assumption originally made of a fully detached flow dominated by geometry sharpness (mainly the bilge keels). The importance of the boundary layer mesh is highlighted by this result.

INFLUENCE OF THE MESH GENERATION METHODS

In order to improve the unstructured mesh simulations, P1 studied the influence of the mesh generation methods on the

results. For comparison's sake, the structured mesh is taken as the reference.

Unstructured meshing algorithm

The mesh generation algorithm will mainly influence the cell size jumps. The standard Octree unstructured mesh generation method is very robust with respect to input geometry accuracy and it is also relatively easy to use since it is mostly automated. Its main drawback lies in the large cell size jumps between zones with different refinements parameters. If strong flow variable gradients come across these size jumps, it might result in a large numerical dissipation which can greatly affect the accuracy of the computation. The Delaunay mesh generation method is more time consuming to apply since it requires a clean geometry and a good surface mesh of the domain before generating the volume grid. It results in much smoother cell size transitions that can decrease the associated numerical error. In order to check the influence of this effect on the results, two meshes with identical refinement parameters were tested on the 90° heading. They both featured the extended refinement box mentioned in the previous paragraph and the high y^+ boundary layer mesh. Midship mesh planes are shown in Figure 11.

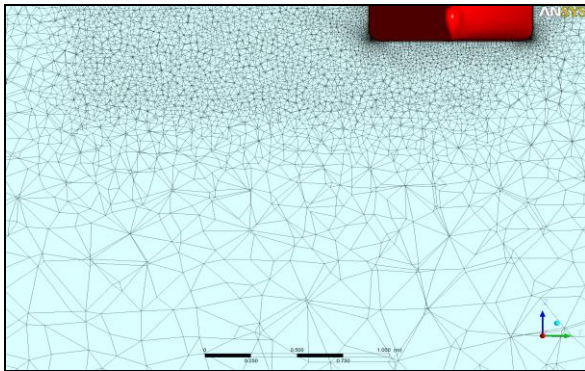


Figure 11 – Midship plane for the Delaunay mesh

Table 8 - Mesh sizes and computed loads for the mesh generation method comparison

Mesh type	mesh size(nodes)	Fy	y^+ (Mean/Max)
Octree: Standard mesh	2,821,913	0.878	0.9 / 1.42
Octree: Large refinement box with high y^+	2,800,899	0.820	8.5 / 17.5
Delaunay: Large refinement box with high y^+	2,656,818	0.808	8.2 / 15.8
Structured mesh	3,080,502	1.017	0.7 / 0.9
Model test	-	1.000	-

As shown in Table 8, the difference in the loads computed with the two meshes generated by Delaunay and Octree methods is marginal and less important than the effect of the boundary layer mesh coarsening. Flow visualizations not showed here lead to a similar conclusion from a more

qualitative point of view. It appears therefore that using the Delaunay method does not lead to significant simulation differences while costing additional engineering effort.

Boundary layer mesh height

As shown in the vorticity contours in Figure 12, the flow at head current mostly remains attached to the hull. This boundary layer type of flow requires a specific attention to the quality of the boundary layer mesh. For unstructured meshes, the boundary layer is captured with an inflated layer of prismatic elements. The transition from prisms to tetrahedrons is ensured mostly with pyramid elements. These elements are notoriously numerically diffusive and they should be placed outside of the boundary layer. In other words, the prism layer height must be higher than the physical boundary layer to avoid excessive numerical dissipation. The cost of an increase of the boundary layer mesh height is relatively low since for an expansion factor of 1.25, adding about 3 layers will more than double the height. For the 180° case, two different Prism layer mesh height are tested and the result is checked against the structured mesh computation which does not suffer this issue since only hexahedral elements extending far outside the boundary layer are used with a controlled expansion factor. Figure 13 compares the boundary layer profiles obtained with the different meshes. In this graph, the boundary layer limit is defined as the surface for which the longitudinal velocity component is 95% of the free stream velocity. The comparison shows that boundary layer mesh truncation has a clear effect on the flow impairing the boundary layer growth. It also shows that when the physical boundary layer is completely contained within the prismatic layer, its profile is very similar to what is obtained with the structured mesh.

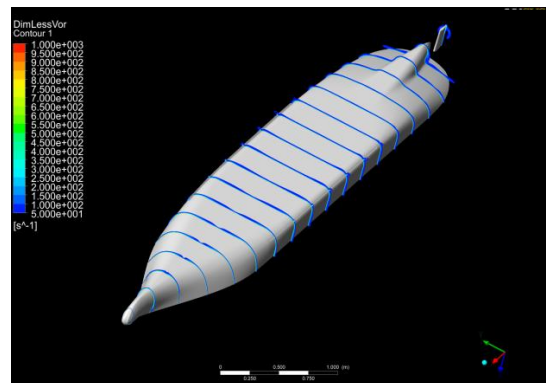


Figure 12 – Vorticity contours for the 180° heading

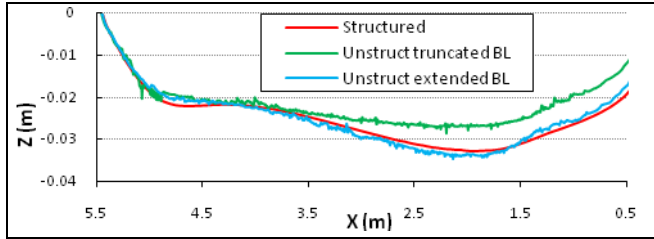


Figure 13 - Boundary layer profiles for the different simulations at the centerline plane along the hull

Comparing the drag forces in Table 9, one sees that it is mostly the shear forces which are affected by the boundary layer mesh truncation. Indeed, these are the most sensitive to the boundary layer modeling. While the structured mesh and unstructured mesh with extended boundary layer mesh give very close drag forces, the truncated boundary layer results in a 7% difference for the friction drag.

Table 9 - Computed drag forces for the different boundary layer treatments

Case	mesh size (nodes)	$F_{x_{pressure}}$	$F_{x_{friction}}$	$F_{x_{total}}$
Model test	-	-	-	1
Steady structured	2,530,812	0.107	0.683	0.790
Steady unstructured truncated BL	2,821,913	0.107	0.639	0.747
Steady unstructured extended BL	2,932,337	0.105	0.690	0.795

MODELING VARIATIONS

Besides purely numerical aspects, the influence of the modeling parameters on the simulation results was also studied by the participants. Turbulence and boundary conditions were considered in these studies.

Turbulence Model variation

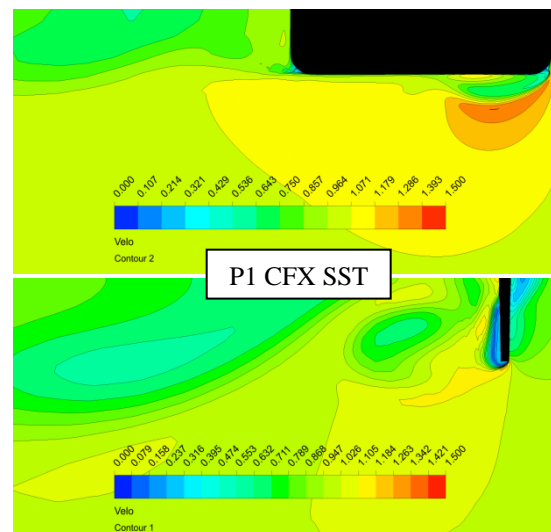
The turbulence model is an important aspect of the RANS formulation. Its influence on the current loads which can be significant was assessed by P1. For the 135° headings, different turbulence models were tested on the same structured mesh. The first is the linear eddy-viscosity SST model which is Menter's improved version of the standard $k-\omega$ model [13]. It is a widely used RANS model in the industry and considered as very robust in terms of application range. The swirling detached flows expected downstream of the bilge keels and the bow are better modeled with an anisotropic treatment of turbulence. For this reason, the non linear Baseline Explicit Algebraic Stress Model (BLEASM) was also tested. It is also a two equation model derived as an explicit solution of the Algebraic Stress Model proposed by Rodi [14]. The CFX implementation is based on the formulation by Hellsten [15] and Wallis and Johansen [16]. Although, it is also a two equation model, its equations are stiffer and therefore more difficult to solve numerically than SST. A step further in complexity is achieved with the Reynolds Stress Model (RSM) which solves the transport of the complete Reynolds Stress tensor coupled with

an equation for the transport of the turbulent dissipation frequency ω . The ω equation is based on the baseline turbulence model. In total, RSM amounts to the resolution of 7 transport equations which makes it computationally intensive as well as theoretically more accurate model than the previous eddy viscosity models. The last model to be tested was Menter's Scale Adaptive Simulation (SAS). This 2-equation model based on the transport of the Von-Karman length [17] offers a hybrid approach to turbulence modeling. Depending on the local turbulent scale, it switches from a classical SST model to a LES type of sub-grid modeling. This approach similar to DES requires a time dependant simulation. The computational requirements are therefore tremendously increased. Table 10 shows the main force component for the different simulations.

Table 10 - Computed forces for the different turbulence models at the 135° heading

Turbulence model	F_y
SST	0.805
BLEASM	0.826
RSM	0.836
SAS	0.834

The differences in computed loads between the models are relatively low but the trends show an increase in the force with respect to the complexity of the turbulence model. The velocity contours at the midship plane and the rudder plane are given in Figure 14. The complexity of the flow can be observed in the resolved scales. In the absence of detailed flow measurements, validation is not possible. However, the advanced RSM and SAS models bear remarkably similar results which are clearly different results from other the eddy viscosity models. The SST model seems to underpredicts the bow and bilge keel vortices. This difference is observed for the computations from both participants. The BLEASM model shows a slightly better resolved flow field. However, the intensity of the captured eddies are weaker than for RSM and SAS.



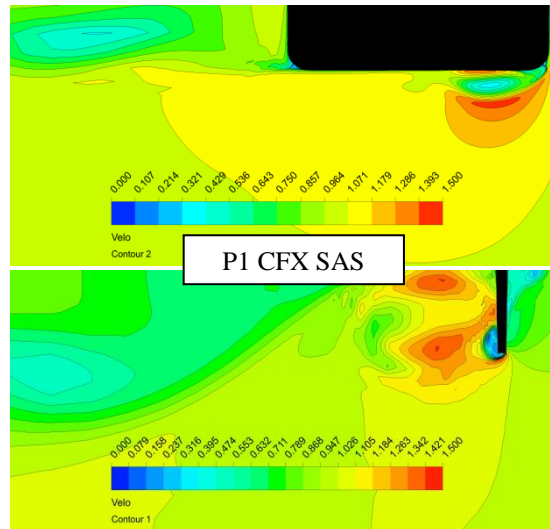
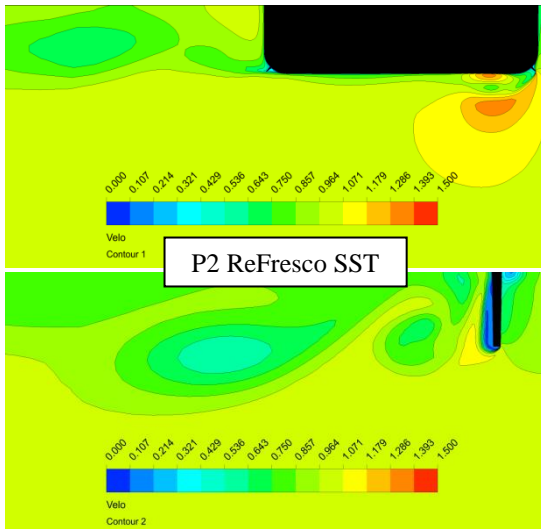
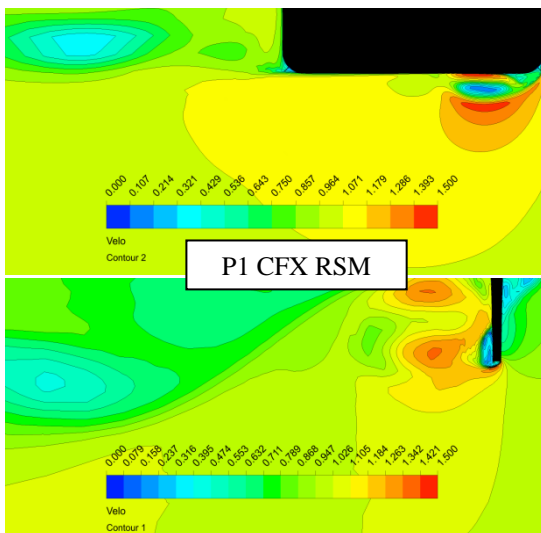
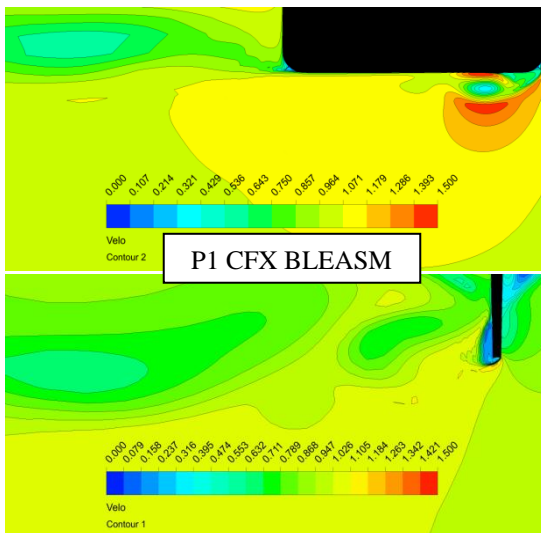


Figure 14 – Midship and rudder plane wake profiles for the different turbulence models at 135⁰ heading.



The differences observed in the velocity fields result in relatively small global loads discrepancies while the additional calculation time required by RSM or SAS is significant. If one is interested in the flow details, for instance in order to characterize the propeller inflow, these advanced models are most suited. On the other hand, if one is only interested in the global loads, the differences observed here do not justify the additional effort required for advanced turbulence modeling. It could be used instead to improve the mesh resolution and try to reach a grid independent solution. The BLEASM model seems to bring a small improvement of the vortex modeling for a relatively low additional computational cost when compared to the SST model.

Study of blockage effect

P2 studied the effect of flow blockage by varying the bottom wall boundary condition of the cylindrical domain. Originally set as a constant pressure opening, it was changed into free slip wall. The wall condition forces a constant mass flow rate between the inlet and the outlet thereby increasing the pressure on the hull. The quantification of this blockage effect which is highly dependent on the basin dimensions helps characterizing the representativity of the measurements. The study was done for the 140⁰ heading. A grid dependence study was performed with the blocked flow for two different grid sizes. The results are presented in Table 11. They exhibit a relatively limited grid dependence of the results.

Table 11 Mesh refinement study for the GridPro meshes at 140⁰ with bottom wall boundary condition

	Coarse	Fine
Grid size	2 173 415	4 367 719
F _y	0.907	0.906
ε	-	-1.32%

Table 12 Comparison of the lateral drag at the 140° heading for the different set-up used by P2

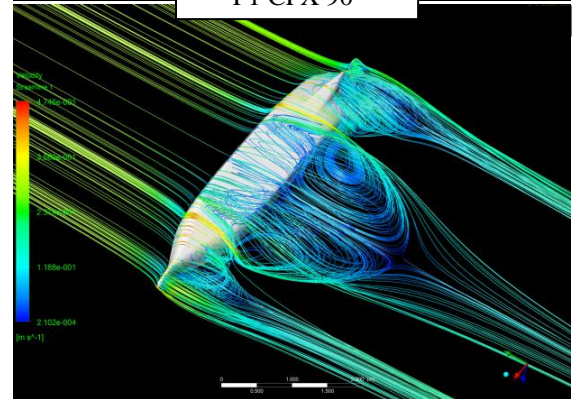
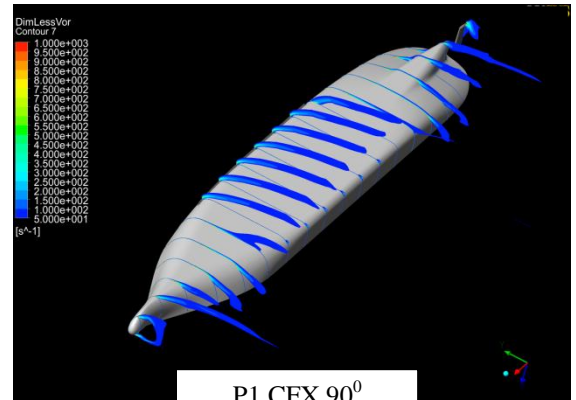
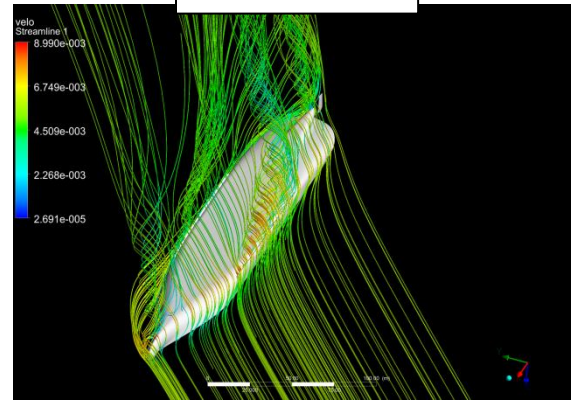
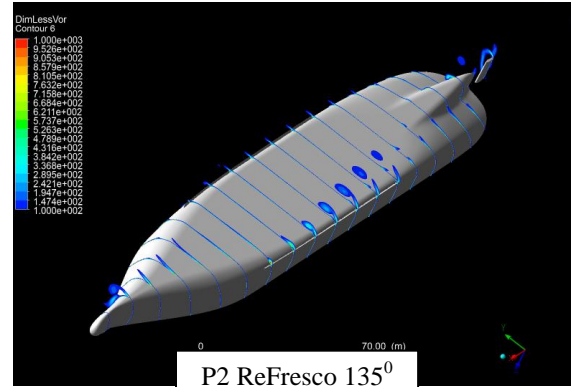
Case	Domain	Fy
CFX – ICEM mesh	Basin dimensions	0.923
ReFresco – ICEM mesh	Basin dimensions	0.905
ReFresco – GridPro mesh	Cylindrical domain with wall at bottom boundary	0.906
ReFresco – GridPro mesh	Cylindrical domain with opening at bottom boundary	0.719

The forces from the various setups are compared in Table 12. They show that the blockage effect due to the bottom wall results in a significant increase of the drag forces of about 25%. On the other hand, the presence of the side walls has little influence on the results. No measurements without blockage are available for validation. However, the small grid-dependency and the good agreement for the case with blockage suggest that the CFD results are reliable. The ability to predict blockage effects is seen as a key feature of CFD application in maritime engineering. The reliable quantification of blockage effects using CFD deserves further study and will be taken on in future work.

RESULTS FOR ALL HEADINGS

Flow description

Following the numerical verifications, the flow simulations were carried out for all headings by each participant. Depending on the heading, different types of flow are encountered. In spite of the differences between the results from different set-ups, some general flow features can be characterized. As shown in Figure 12, at 180° the boundary layer remains mostly attached to the hull. The influence of the bilge keels on the flow is negligible and the current forces are therefore dominated by friction. Vorticity contours and flow streamlines are shown in Figure 15 for head quartering and beam and stern quartering current. For angles deviating from head current, flow detachment is initiated at the sharp edges and high curvatures of the geometry such as the bilge keels, the rudder and the bulb. For quartering current, longitudinal vortices are generated and transported along the main flow direction. The loads are dominated by pressure forces on the hull. This is also the case for beam current where large recirculations are initiated at the bilge keels. These large vortices transverse to the flow direction remain attached to the hull. For stern quartering currents, large longitudinal vortices are initiated at the skeg and the bilge keels.



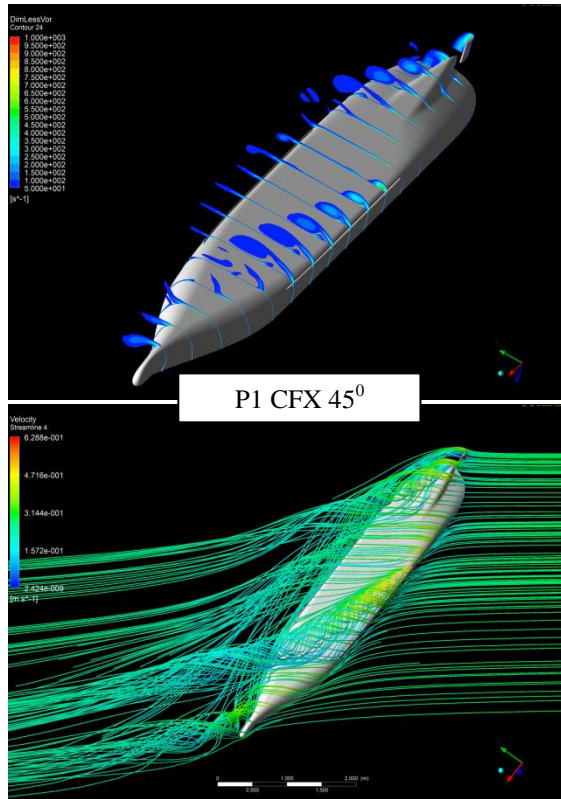


Figure 15 – Vorticity contours and flow streamlines for different set-ups

Comparison of the current loads

The following set-up have been used for all the headings:

- CFX: Steady computation with ICEM unstructured mesh (P1)
- CFX: Steady computation with ICEM structured mesh (P2)
- ReFresco: Steady computation with GridPro structured mesh and with open bottom boundary condition (P2)

Additionally, the following results are added to the comparison:

- CFX: Unsteady computation with ICEM structured mesh for 3 headings, 180⁰, 135⁰ and 90⁰ (P1)
- ReFresco: Steady computation with ICEM structured mesh for 2 headings 140⁰ and 90⁰ (P2)

Drag, lift and Yaw moment are compared with the model test results for all the mentioned cases in Figure 16. The comparison leads to the following remarks:

- The variety of approaches and computational setups leads to significant variability of the resulting loads.
- All the different simulation setups exhibit similar evolution trends of the loads with respect to the heading. These trends are in good agreement with the model tests results.
- Quantitative agreement between the simulated loads and the model tests is in general better for the drag and

lift coefficient than for the yaw moment. This is mostly due to the fact that the force calculation is a direct summation of all the hull element contributions while the moment takes into account the load distribution on the hull which is less prone to error cancellation.

- From all the simulations with bottom basin wall, loads from P1 unstructured simulation present the largest deviation with the model tests. On the other hand, the comparison of P1 results with structured mesh shows a good agreement with the measurements. This agreement is even improved for the structured mesh with unsteady simulation. These observations are consistent with the improved numerical accuracy of flow aligned hexahedral elements when compared to tetrahedrons.
- For the P2 results the best agreement is obtained with CFX on the ICEM grid which respects the basin dimensions. The comparison on this same grid between the CFX and ReFresco shows relatively close results.
- ReFresco results with open bottom give significantly reduced loads. This reduction due to the absence of blockage effect is present for all headings.

The comparisons show that CFD can efficiently estimate the current loads on the hull for all headings. It also gives valuable physical information on the flow. It notably helps characterizing the influence of blockage from the basin. The effect of the different hull appendages on the flow can be visualized and quantified. While different types of simulation set-up can have different costs, they also lead to different result. Advanced modeling such as time dependent simulation and RSM or SAS turbulence model are computationally demanding. In terms of engineering effort, generating structured mesh generation involves more work than unstructured meshing. It appears through the comparisons made during this project that most of these additional costs are rewarded with a better accuracy and a better confidence in the results. For efficiency purposes, a balance has to be found between cost (computational and engineering) and the required accuracy. The different comparisons presented here are meant to be used as starting consideration point for this question.

CONCLUSION

A number of CFD Current simulations were performed within the JIP Current Affairs. The case of a LNGC hull simulated by two different participants has been presented in this paper. Different modeling approaches were tested and comparison was made with the towing test measurements. The feasibility and relative accuracy of the simulations have been studied through numerical studies. The differences between different types of meshing techniques and type of mesh refinement were highlighted. Some of the modeling assumptions were also studied by varying the turbulence model and the boundary conditions. The mesh convergence studies

showed that for the structured meshes, grid dependency of the loads was not significant. However, the general comparison between the results from the different setups exhibits variability on the computed loads.

This research showed that CFD is an efficient tool to assess current loads. It also showed that for reasonably large grids the quality of the results is still largely influenced by the user set-up. The numerical and modeling issues covered in this paper were neither completely exhaustive nor explored in their full depth. However, the objective here was to bring awareness on their existence to the JIP participants and get a feel for their potential implications in terms of current load computations. The results presented here were successfully used in combination with other JIP deliverables to produce a set of guidelines for the assessment of current loads with CFD.

The JIP has come to its term but the cooperation model promoted will remain in the form of future joint research projects between the participants. Further work should include the use of larger meshes and a comprehensive study on the effect of unsteadiness in combination with local flow measurements. From there, additional modeling assumptions can be explored with CFD such as the laminar-turbulent flow transition and influence of the water free surface.

ACKNOWLEDGMENTS

The following participants in the Current Affairs JIP are acknowledged; Amog Consulting, Petrobras, SBM Offshore, Projemar, Heerema, Statoil Hydro, Keppel Fels, Total, INTECSEA and MARIN. The authors would also like to thank Guilherme Vaz for his contribution to the project and his valuable comments on the paper.

REFERENCES

- [1] van Walree, F., and van den Boom, H.J.J. "Wind, Wave and Current Loads on Semi-Submersibles". OTC1991-6521, 1991.
- [2] Vaz, G, Waals, O. J., Ottens, H., Fathi, F., Le Souef, T., Kiu, K., "Current Affairs: Model Tests, Semi-Empirical Predictions and CFD Computations for Current Coefficients of Semi-Submersibles". OMAE2009-80216. Honolulu, Hawaii, USA. 2009.
- [3] Larsson, Stern Bertram, "Benchmarking of CFD for Ship Flows: The Gothenburg 2000 Workshop," J. Ship Research, Vol. 47 No. 1, March 2003, pp. 63-81
- [4] Takanori Hino (editor), "CFD Workshop Tokyo", March 9-11 2005, National Maritime Research Institute
- [5] Jurgens, A.J., Hallmann, R. and Tukker, J., "Experimental investigation into the flow around a manoeuvring LNG carrier on shallow water", NAV 2006 International Conference on Ship and Shipping Research
- [6] Olaf Waals (MARIN), "On the Application of Advanced Wave Analysis in Shallow Water Model Testing (Wave

Splitting)", OMAE2009-79413, OMAE Conference, Honolulu, June 2009

[7] Cozijn, H., Motions and Mooring Loads of an LNG-Carrier Moored at a Jetty in a Complex Bathymetry, OMAE2009-79420, Honolulu, Hawaii, USA. 2009.

[8] L. Eca and M. Hoekstra, "On the numerical verification of ship stern flow calculation", Proceedings of the 1st MARNET Workshop, Barcelona, Spain, 1999

[9] ITTC 1999, Proceedings of the 22nd International Towing Tank Conference, Seoul, Korea / Shanghai, China, 1999

[10] M. Casey and T. Wintergerste (editors), "Best Practice Guidelines", ERCOFTAC Special Interest Group on Quality and Trust in Industrial CFD, 2000

[11] ANSYS Inc., ANSYS CFX11.0 Users Manual, 2008.

[12] Toxopeus, S., and Vaz, G. "Calculation of Current or Manoeuvring Forces using a Viscous Flow Solver". OMAE2009-79782. Honolulu, Hawaii, USA. 2009.

[13] Menter, F. "Two-equation Eddy Viscosity Turbulence Models for Engineering Applications". AIAA Journal, 32, pp. 1299-1310, 1994.

[14] Rodi, W., "A new algebraic relation for calculating the Reynolds stresses". ZAMM 56: 219-221, 1976.

[15] Hellsten, A. "New advanced k-w turbulence model for high-lift aerodynamics". AIAA paper 2004-1120, Reno, Nevada. 2004.

[16] Wallin, S., and Johansson, A., "A complete explicit algebraic Reynolds stress model for incompressible and compressible flows". Journal of Fluid Mechanics, 403, pp. 89-132, 2000.

[17] Menter, F. R., and Egorov, Y. "A Scale-Adaptive Simulation Model using Two-Equation Models". AIAA Journal, 1095, 2005.

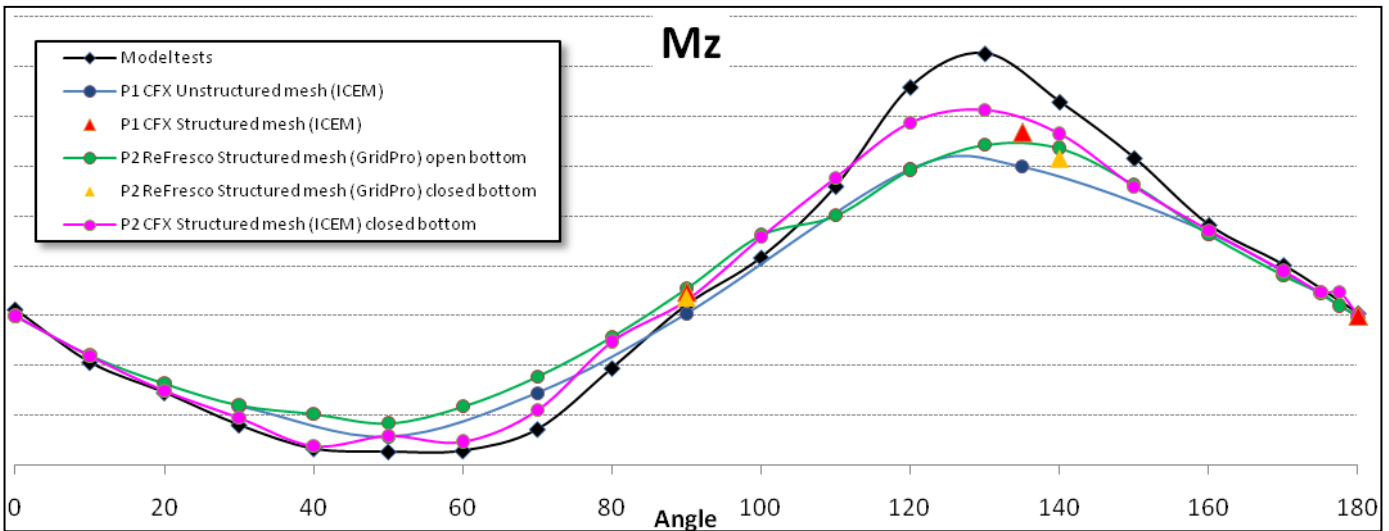
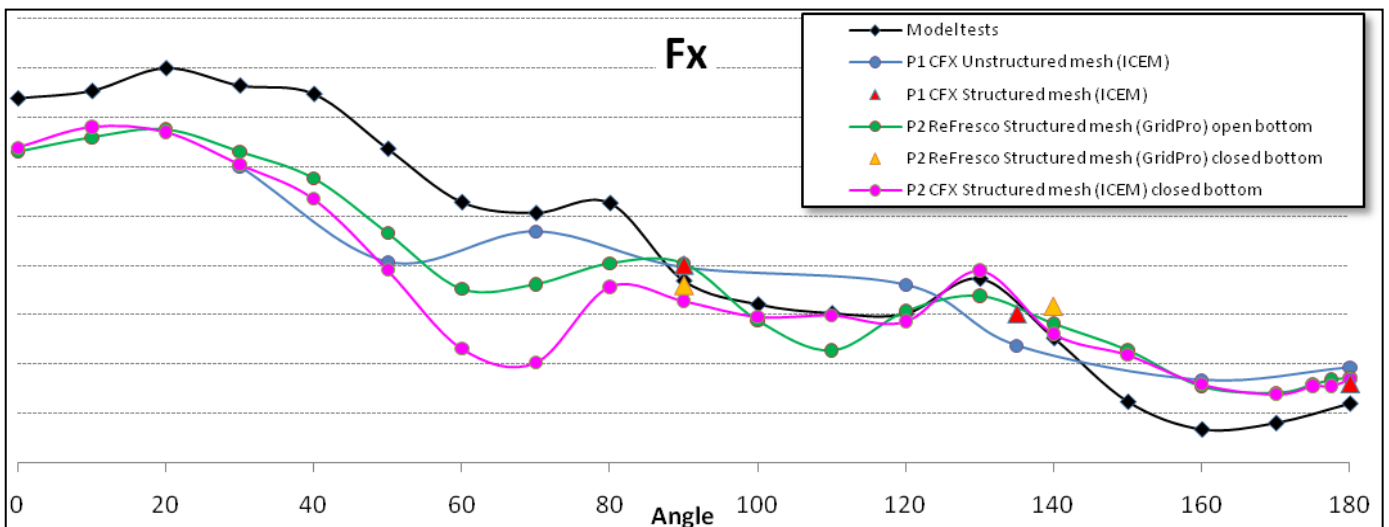
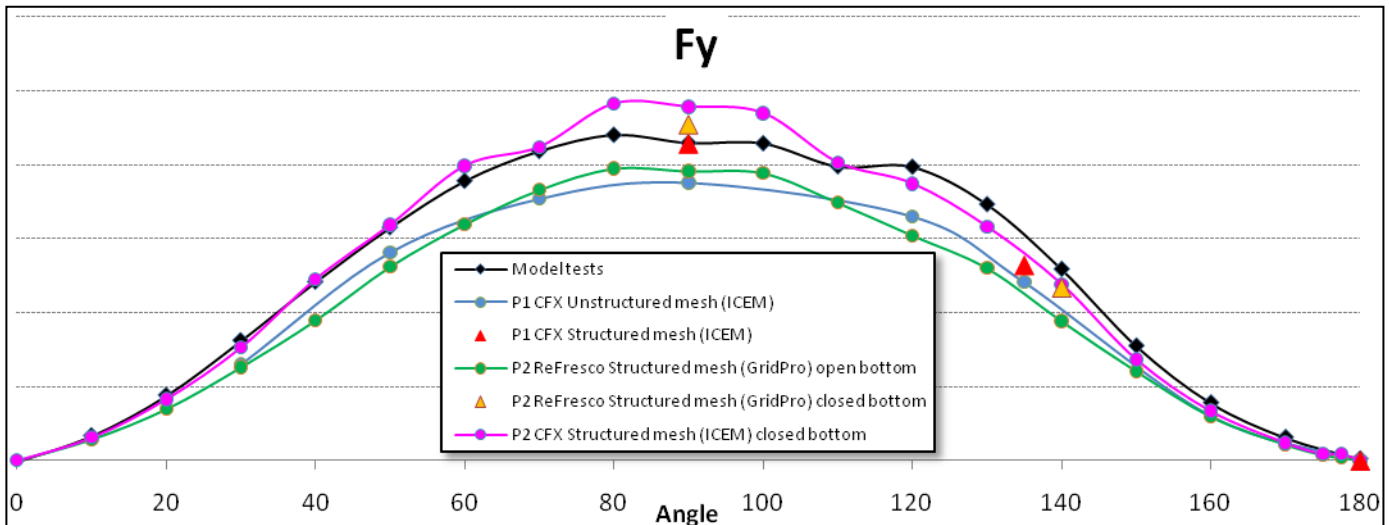


Figure 16 – Lift, Drag and Yaw moment comparison between different CFD calculations and the model tests at all headings